Effect of acid-treatment and colloidal-processing conditions on the room temperature mechanical and electrical properties of 3YTZP/MWNT ceramic nanocomposites

R. Poyato[1,2], A. Morales-Rodríguez[1,2], F. Gutiérrez-Mora[1,2], A. Muñoz[2], Á. Gallardo-López[1,2].

1. Inst. Ciencia de Materiales de Sevilla (CSIC-US). Américo Vespucio 49. 41092 Sevilla. Spain.

2. Dpto. de Física de la Materia Condensada. Univ. de Sevilla. Apdo. 1065. 41080 Sevilla. Spain.

Abstract

Different colloidal powder processing routines have been used to prepare composites of 3 mol% Y_2O_3 -ZrO_2 (tetragonal zirconia polycrystals, 3YTZP) with 2.5 vol.% multiwall carbon nanotubes (MWNT) with the aim of achieving a homogeneous distribution of the MWNTs in the ceramic, eliminating agglomerates but also minimizing carbon nanotubes (CNTs) damage during processing. Modifications of the acid treatment applied to the nanotubes, including subjecting them to stirring or ultrasonic agitation, and use of acid or basic pH during composite powder mixing have been approached.

No MWNT damage during processing was detected by Raman spectroscopy. CNTs bundles were found in all the composites forming different patterns depending on the processing route. Similar values of hardness were obtained for all the composites, while different anisotropy in fracture propagation was found when studying parallel and perpendicular directions to the sintering pressing axis on the cross sections of the composites due to the MWNT preferential alignment. The CNT bundles were found to act as fracture short paths. A similar anisotropic behavior was observed for the electrical conductivity. These results have been correlated to the different microstructures obtained in the composites prepared with different processing routines.

1. Introduction

For more than two decades, the scientific community has paid great attention to carbon nanotubes (CNTs) which have remarkable Young´s modulus (up to 1.2 TPa), strength, chemical and thermal stability and outstanding resilience. These attractive properties have motivated many researchers to focus on ceramic composites containing CNTs with the aim of improving the properties of the matrix.

Nowadays, the development of industry and society requires composite materials possessing not only excellent mechanical properties but also outstanding functional properties[1]. However, despite the outstanding properties and functionalities of the CNTs, their chemical inertness and their entangling due to van der Waals forces hinder the fulfilment of their potential benefits on these composites. Non-uniform dispersion of CNTs can result in the presence of large agglomerates and poor densification[2-4]. Thus, composite powder processing and consolidation are key points in order to achieve fully dense composites with homogeneous CNT distribution through the ceramic matrix.

Several processing approaches have been proposed in literature. Physical mixing under wet conditions by ultrasonication or ball milling[5-7], and in-situ growth of CNTs on the surface of ceramic powders[8,9] were proposed by different authors. More recently, other researchers focused on the incorporation of chemically modified CNT into the ceramic matrix with the aim of improving the surface compatibility of the CNTs with the host matrix. Both covalent and non-covalent functionalization of CNTs have been investigated in order to modify the inert hydrophobic CNT surface[2,10,11]. Although other attempts such as oxidation in air or basic etching have been approached[10], acid treatment of CNTs is one of the more widely used methods for covalent functionalization[2,12-17]. The rationale behind this technique is the shortening of the CNTs and the formation of carboxyl groups on their surfaces[15] when dispersed in aqueous media, resulting in a highly stabilized suspension due to an electrostatic effect[2], which would facilitate the homogeneous dispersion of the CNTs in the matrix. Also, an enhancement of mechanical interlocking with the ceramic matrix is expected as a consequence of the chemical surface roughness created by the attaching of functional groups to the CNTs surface. Acid treatments by reflux of the CNT-acid mixture[11-13], by

mechanical stirring[10,16] or ultrasonication[12,15] of this mixture, with different temperatures[16] or times[10], have been studied searching for an enhancement of the benefits while avoiding damage to the CNTs.

The colloidal method is considered one of the most effective means of homogeneously incorporating chemically modified CNT suspensions into a ceramic matrix. Although some authors prepared the acid-treated CNTs/ceramic particle slurry just by magnetic stirring in ethanol[14,15], other groups proposed advanced colloidal techniques including pH control. Estili et al[12,13] and more recently Wang et al[16] proposed colloidal processing at acidic pH to prepare Al_2O_3/MWNT composites. In these conditions, the CNTs and the ceramic particle surfaces are negatively and positively charged, respectively, and a flocculation process (also called heterocoagulation process) between them takes place. Other authors proposed processing at basic pH[2,11,17], where the surface charges are both negative and charge stabilization is promoted in the aqueous solution. All these studies attempted surfactant-free processing, as opposed to previous works[18,19] incorporating surfactants to modify the surface charge of the particles and /or CNTs. However, the possibility of incomplete surfactant removal or their effect on the composite properties motivated the avoidance of surfactants.

Even though the advanced colloidal techniques including CNT acid treatment and aqueous solution pH control have been used for several years to prepare Al_2O_3/CNT composites[2-4,11-13], it has not been until recently that these techniques have been applied to the processing of zirconia/CNT composites[14,15,17]. Yi et al[14,15] sonicated multiwalled carbon nanotubes (MWNTs) at 40ºC in sulphuric acid and dispersed the MWNTs and zirconia particles in ethanol under magnetic stirring, followed by ultrasonic agitation. Kasperski et al[17] submitted double walled carbon nanotubes (DWNTs) to a soft functionalization at room temperature using a mixture of nitric, sulphuric and chloridric acids and used basic pH to disperse the zirconia and DWNT mixture. Both studies described a decrease in hardness and an increase in electrical conductivity for CNT contents up to 4.5 wt%.

In this study, we have prepared 3YTZP composites with 2.5 vol.% MWNT by spark plasma sintering of powders prepared using different colloidal processing routines, with the main objective of differentiating the benefits or disadvantages of each

of them in terms of optimizing MWNT distribution through the ceramic matrix. These processing routines include subjecting the MWNTs to two different acid treatments and ulterior composite powder mixing in aqueous solution with either basic or acid pH. The effect of each routine on the composite microstructure, hardness, fracture behavior and electrical conductivity has been analyzed.

2. Experimental procedure

2.1. Materials processing

2.1.1. MWNT acid treatment

Commercially available purified MWNTs (Nanolab Inc., Waltham, MA, USA) with 1-5 μm length and average external diameter 15 ± 5 nm (supplier data) were selected as starting material. The acid treatment of the MWNTs was carried out using a mixture of concentrated sulphuric acid (98%) and nitric acid (70%) in the ratio 3:1, with the aim of disentangling and cutting the raw MWNT ropes. Two different set of conditions were used. In the first one, the MWNTs were suspended in the acid mixture for 2 h under magnetic stirring (referred to as MWNT-ST). In the second one, the MWNTs were suspended in the acid mixture and subjected to ultrasonic agitation by means of an ultrasonic bath (240 W) for 2 h (referred to as MWNT-US). Both processes were carried out at room temperature. The acid-treated MWNTs were collected on ~20 nm pore filter membranes, washed in high purity ethanol for several times and freeze-dried in order to avoid possible re-agglomeration.

2.1.2. 3YTZP/MWNT powder colloidal processing

The 3 mol% yttria stabilized tetragonal zirconia powder (3YTZP), with 40 nm particle size and 99% purity, was obtained from a commercial source (Nanostructured and Amorphous Materials Inc., Houston, TX, USA). The colloidal processing of the 2.5 vol.% 3YTZP/MWNT composite powders was carried out in aqueous solution following two different routines. In both cases, the use of surfactants that could introduce undesirable impurities which could affect the sintering process and/or the composites' properties was avoided. In the first routine, a basic charge stabilization

technique described elsewhere2 was followed. In a first step, the ceramic powder and the MWNTs were independently suspended in a highly basic aqueous solution (pH= 12), where both their surfaces are negatively charged, and subjected to ultrasonic agitation for two different times (15 or 45 min) by means of a high power ultrasonic probe (Model KT-600, Kontes Inc., Vineland, NJ) at 20 kHz and 95% amplitude. In a second step, the composite powder blends were mixed in aqueous solution and subjected to ultrasonic agitation for 5 min. The composite slurry drying was carried out by using a hot plate at 80°C with continuous stirring. In the second routine, a heterocoagulation technique[16] was followed. In this case, the ceramic powder and the MWNTs were independently suspended in acid aqueous solution (pH = 5.2), where their surfaces have opposite charges, and subjected to ultrasonic agitation for 15 min by means of an ultrasonic probe. In a second step, the suspensions were gently mixed by introducing the MWNT suspension into the ceramic powder suspension, and then vigorously stirred. When magnetic stirring of the suspension was finished, the flocculation process between the MWNTs and the 3YTZP particles started immediately and it was considered completed once the supernatant became transparent. The slurry was immediately frozen by immersion in liquid nitrogen and subsequently dried by lyophilization at -80 °C using a Cryodos 80 lyophilizer. Nylon filters were used in order to avoid composite powder loss during the process.

The different processing routines used to obtain the composite powders are summarized in Table 1. Notation of the composites includes information about the corresponding routine: stirring/ultrasonic agitation during acid treatment (ST/US) and charge stabilization/heterocoagulation technique (stab/het). Information about tip sonication time is included only in the notation of the composite prepared using ultrasonic agitation for 45 minutes.

2.1.3. Spark Plasma Sintering (SPS)

SPS (Model 515S, SPS Dr Sinter Inc., Kanagawa, Japan) was used to sinter the materials in a 15 mm diameter cylindrical graphite die/punch setup in vacuum. All the composites were sintered at 1250 °C for 5 min under 75 MPa with 200 °C/min heating and 50 °C/min cooling ramps. A sheet of graphite paper was placed between the powders and the die/punches to ensure their electrical, mechanical and thermal contact.

A graphitic paper was also placed along the inner wall of the die for easy removal of the sample. The temperature was measured by means of an optical pyrometer focused on a bore hole in the center of the graphite die. The sintered composites of ~15 mm in diameter and ~2 mm in thickness were ground to eliminate the surface graphite.

The density of the sintered composites was measured by the Archimedes method using distilled water as immersion medium. The theoretical density of the composites, ρ=6.0 g·cm^{-3}, was calculated using the rule of the mixtures, considering ρ=6.1 g·cm^{-3} for 3YTZP and ρ=2.1 g·cm^{-3} for the MWNTs.

2.2. Microstructural characterization.

Phase identification was carried out using X-ray diffraction (XRD, model D8 Advance A25, Bruker Co., MA, USA). The Raman spectra of the as-received MWNTs, the acid-treated MWNTs (MWNT-ST and MWNT-US) and the fracture surfaces of the sintered composites were obtained using a dispersive microscope (Horiba Jobin Yvon LabRam HR800, Kyoto, Japan) equipped with a 20 mW He-Ne green laser (532.14 nm). The microscope used a 100x objective and a confocal pinhole of 100 μm. The Raman spectrometer was calibrated using a silicon wafer. Six to eight spectra were taken for each sample.

Microstructural observations of sintered composites were carried out on fracture and polished surfaces by high-resolution scanning electron microscopy (HRSEM), using a Hitachi S5200 microscope (Hitachi High Technologies America Inc., USA) and a FEI-Teneo microscope (FEI, USA) with the aim to analyze the distribution of the MWNTs in the matrix, and to characterize the ceramic grains morphology. The possible presence of MWNT agglomerates in the composites was analyzed by low magnification conventional SEM using a JEOL 6460LV microscope (JEOL USA Inc., MA, USA). Cross-section (c.s.) and in-plane (i.p.) slices, i.e. surfaces parallel and perpendicular to the SPS pressing direction, were polished with diamond paste up to 1 μm for morphological studies. Additionally, the polished c.s. surfaces devoted to characterize the 3YTZP grains were thermally etched at 1150 ºC for 20 min in air to reveal the grain boundaries. The average grain size of the 3YTZP tetragonal phase was estimated by the

linear intercept method from SEM micrographs, measuring about 300 grains from each composite.

2.3. Mechanical and electrical characterization.

Vickers indentation tests were carried out with a diamond Vickers micro-indenter (Wilson VH1150, USA) under 10 kgf, to estimate hardness at room temperature. At least 15 valid measurements were carried out on mirror-like finished surfaces for each sample, in well-separated and randomly selected regions. The tests were performed on both c.s. and i.p. surfaces. The hardness value, H_V, was calculated from the indentation load, P, and the diagonal of the Vickers imprint, a.

$$H_V = 1.854\left(\frac{P}{a^2}\right) \quad (1)$$

The crack fracture lengths starting from the corners of the Vickers imprints were measured in order to analyze the crack propagation. At least 15 imprints for each composite were evaluated for statistical purposes.

The electrical conductivity was estimated using the capacitive method (metallization of two faces of the sample and measurement between the two electrodes). The measurements were performed on parallelepiped specimens at room temperature with direct currents using a model 2000 Keithley multimeter. A colloidal silver paste was applied on both sides of the samples and the electrodes were fired at 600 ºC for 30 min under argon flow to avoid degradation of the MWNTs during the process. Two different electrode configurations were used to measure the conductivity in the directions parallel ($\sigma_{\parallel}$) and perpendicular ($\sigma_{\perp}$) to the SPS pressing axis.

3. Results and discussion.

3.1. Microstructure.

The XRD patterns of the sintered composites are shown in Fig. 1. In all the samples it is clear the presence of the zirconia tetragonal phase (JCPDS 01-078-1808) as the main one, with a contribution of the zirconia monoclinic phase (JCPDS 01-081-

1314, main peaks at 2θ = 28.2 and 31.4º). No remarkable differences were observed on the amount of the secondary monoclinic phase in the composites prepared using the different processing routes. The existence of this secondary phase in the 3YTZP matrix has been related to the presence of the CNTs surrounding the 3YTZP ceramic grains. It has been published that the transformation from the tetragonal to the monoclinic phase during cooling after SPS can be promoted by an increase in the CNT content[20] or by improving their dispersion in the case of composites with the same CNT nominal content[21,22].

In the XRD pattern corresponding to the composite prepared with MWNTs subjected to tip-sonication for 45 minutes a peak at 2θ = 26.6º is observed, which corresponds to the main peak of graphite (JCPDS 00-026-1076). Thus, it can be concluded that sonicating the CNTs with the high energy probe during such a long time has damaged them. It has been previously reported that long time sonication can not only enhance dispersion of CNTs but it can also induce defects and even scission of the tubes[23]. This composite was not further analyzed.

Possible structural defects generated on the MWNTs during the acid treatment or spark plasma sintering were evaluated by Raman spectroscopy. The spectra corresponding to the as-received and acid-treated MWNTs, and to the sintered composites are shown in figures 2 and 3, respectively. The intensity ratio of the MWNTs characteristic peaks D and G (situated in the 1200-1700 cm^{-1} range), I_D/I_G, was calculated from the spectra. A high ratio is usually regarded as evidence of structural defects in the CNTs, as D-Band is usually associated to disordered graphite and crystalline defects[20]. The high ratio observed for the as-received MWNTs (I_D/I_G=0.95 ± 0.06) points to the existence of a non-negligible amount of defective CNTs, although it is not as high as previously published values[11,14]. No significant change in the I_D/I_G ratio is observed for the acid-treated MWNTs (1.03 ± 0.01 for ST and 0.86 ± 0.17 for US), revealing no further deterioration of the CNT structure during the acid treatment. Regarding the sintered composites, remarkable changes of I_D/I_G ratio are not observed either (Table 2), so it can be concluded that neither the acid treatment nor the SPS process induce significant damage to the MWNTs. Some variability in the I_D/I_G values has been observed (minimum and maximum values shown in Table 2). However, it is not as significant as the wide variability reported by previous works, which related this effect to an uneven damage of the CNTs or to the presence of CNT agglomerates, which

would alter the homogeneity of the composites[17-22]. A ~10-15 cm^{-1} shift towards higher frequencies is observed in the G-Band position for the sintered composites when comparing with its position for the as-received and acid-treated MWNTs. This fact has been attributed to compressive strains imposed to the MWNTs by the ceramic matrix[24].

The ceramic grain size in the different composites, together with the density values, are shown in Table 2. Relative densities higher than 97% and similar mean grain sizes (~210-230 nm) were observed in all the composites regardless the different processing routines used. HRSEM images of fracture surfaces of the studied composites are shown in Fig. 4. It can be observed that all the composites present highly densified microstructures with very low porosity. Using this high magnification it is possible to observe MWNT bundles or small MWNT accumulations located at the ceramic grain boundaries. It can also be observed the intergranular character of the fracture mode and a similar grain size in all the composites.

Low-magnification SEM micrographs (Figs. 5a-d) illustrate the MWNT distribution into the ceramic matrix in the polished c.s. surfaces of the composites. The microstructural characterization of ceramic/CNT composites by BSE (backscattered electrons) has been shown to be the most direct method to evaluate the CNT dispersion[2,22]. The presence and distribution of CNT bundles and agglomerates can be clearly visualized because of the high contrast due to the average atomic number difference between the ceramic 3YTZP matrix and C on CNTs. Figures 5a-d show a general view of the composites polished surfaces, whereas Figures 5e-h show details at higher magnifications on these surfaces.

It is highly remarkable that some large MWNT agglomerates (arrowed in Fig. 5d) can only be found in the composite prepared with MWNTs subjected to an ultrasonic bath during the acid treatment and processed by heterocoagulation. The microstructure of this composite is thus composed of areas with dark MWNT bundles distributed throughout the matrix together with some large agglomerates (up to ~40 μm long). Most of these agglomerates appear elongated and preferentially oriented in the direction perpendicular to the SPS compression axis, as it has been previously reported[2,22,25]. These results suggest that the processing routine used to prepare this composite is not adequate to achieve the goal of obtaining an optimized and agglomerate-free microstructure. Although some processing steps that have been shown

to be highly convenient to achieve this goal[21,22], such as MWNT liophilization after the acid treatment or the use of a high energy ultrasonic probe to disperse the CNT suspensions, have been included in the routine, the combination of these techniques with the heterocoagulation of the CNTs and the ceramic particles does not lead to the desired result for the composite US-het.

Hardly any agglomerates are observed in the microstructure of the rest of studied composites, where most MWNTs appear as dark bundles homogeneously distributed within the matrix (Figs. 5a-c). Thus, the processing steps consisting of liophilization after the acid treatment to avoid CNT re-agglomeration and the use of a high energy ultrasonic probe to enhance the CNT dispersion have led to the desired agglomerate-free microstructures. This result was previously published for ceramic composites with low SWNT content[22]; however, the presence of CNT agglomerates was reported for composites with SWNT contents similar to the one used in the present work when the processing conditions were not appropriate[2].

Another observed microstructural feature is the presence of some preferential orientation of the MWNT bundles in the direction perpendicular to the SPS compression axis in the composite ST-stab (Fig. 5a). No similar effect was observed by conventional SEM inspection in the rest of the composites.

It is important to note that the composites prepared with the MWNTs subjected to stirring during the acid treatment show a patterned microstructure when observed at higher magnification (Figs. 5e and 5f). In these composites, the MWNT bundles are distributed surrounding circular CNT-free regions of 10-20 μm size which comprise groups of several ceramic grains. Although no quantitative measurements on the MWNTs depleted regions have been performed, it is clear from the micrographs that the size of the CNT-free regions in ST-het composites is larger (Fig. 5f) than in ST-stab (Fig. 5e). Consequently, the MWNT distribution is better for this latter composite. US-stab and US-het composites (Fig. 5g and 5h) do not show such patterned microstructure. The MWNT bundles are distributed homogeneously through the ceramic matrix but they are shorter than the ones in ST-stab and ST-het composites. In consequence, they do not appear interconnected and surrounding ceramic grains.

3.2. Mechanical properties.

Hardness of the composites is not remarkably dependent on the processing routine, since similar values of H_V were obtained in all the composites (Table 3). Nevertheless, slightly lower values were obtained for the composites prepared with the MWNTs subjected to stirring during the acid treatment. This could point to a better CNT distribution in these composites, as it has been published that lower hardness values are obtained when higher amounts of CNT are located at the grain boundaries, as a consequence of the softer nature of the carbon nanotubes[22]. The hardness values obtained in this work are in the range of the reported values for other 3YTZP/MWNT composites[15,17,26]. No significant differences were observed in the hardness values obtained on the i.p. and c.s. surfaces.

SEM micrographs illustrating typical crack paths generated on the corners of the Vickers indentations carried out on polished c.s. surfaces of the studied composites are presented in Fig. 6. The crack lengths are reported in table 3 for c.s. surfaces, both for directions parallel and perpendicular to the SPS loading axis. Differences in the fracture behavior between the composites prepared with MWNTs subjected to different acid treatment routines and subsequent colloidal processing are found. In the composites prepared with the MWNTs subjected to stirring during the acid treatment, anisotropy in the lengths of the cracks is observed, with longer cracks generated in the direction perpendicular to the SPS pressing axis (Figs. 6a and 6b). This result complements the microstructural feature observed in the BSE images of the composite ST-stab where some preferential orientation of the MWNT bundles in the direction perpendicular to the SPS compression axis was observed (Figs. 5a and 5e). Although this alignment was not clearly detected by means of BSE in the composite ST-het (Fig. 5b), it is clear that it must be present since the anisotropy in the lengths of the cracks is observed also in this composite (table 3). In the composites prepared with the MWNTs subjected to ultrasonic agitation during the acid treatment the anisotropy in the crack length is attenuated when comparing with stirring. A crack length ratio between the perpendicular and parallel orientations of 1.58 is found for the composite US-stab while this ratio is 1.88 for the composite ST-stab. This result clearly indicates an anisotropic mechanical behaviour in these composites, although similarly to the composite ST-het, no clear indication of such anisotropy was found in the microstructural observations (Fig. 5c). This anisotropic effect is not present in the composites prepared with the

MWNTs subjected to ultrasonic agitation during the acid treatment and heterocoagulation (Fig. 5h) nor in the i.p. surfaces of any of the composites (images not shown). In the case of the US-het composite, the lack of anisotropy would point to shorter bundles without significant preferential orientation.

Our results show that the presence of CNTs does not act as toughening element, as it has been proposed by many authors[18,27-29], on the contrary, they act as fracture short paths as it is shown in Fig. 7. As it has been previously stated, a preferential orientation of CNT bundles in the direction perpendicular to the SPS loading axis makes the fracture propagation in that direction easier (Fig. 7a). On the other hand, in the direction parallel to the loading axis, the fracture length shortens due to fracture deviation following a more tortuous path of the unaligned CNT bundles (Fig. 7b). Some of the CNT toughening mechanisms commonly proposed in the literature (CNT bridging, crack deflection and crack pinning) are also present in our composites. In Fig. 7c, a single CNT bundle is shown to act bridging a crack; however, this effect is much weaker than that of the bundles acting as fracture short paths, conferring the composite an overall less tough behavior.

3.3. Electrical properties.

All the studied composites present electrical conductivity higher than 0.3 $S \cdot m^{-1}$ for both $\sigma_{\perp}$ and $\sigma_{\parallel}$ (Table 3), which indicates that the carbon nanotubes content used to prepare the composites (2.5 vol.%) is over the percolation threshold for the two studied directions. This is in good agreement with percolation limits previously published for 3YTZP/SWNT (< 0.4 vol.%[30], < 1 vol.%[21,22]) and 3YTZP/MWNT (< 0.75 vol.%6, < 1.7 vol.%[17], < 2.7 vol.%[15]) composites. In these studies, processing steps such as CNT functionalization[15,17,21], use of surfactants[6,30] or high energy tip sonication[17,21,22,30] during CNT dispersion were incorporated to the processing routine with the aim of obtaining a homogeneous CNT distribution throughout the ceramic matrix. These processing approaches resulted in lower percolation thresholds in comparison with the reported values for 3YTZP/MWNT composites prepared using conventional mixing techniques as ball-milling (~4.7 vol.%)[31,32]. The existence of CNT agglomerates in composites prepared using ball-milling probably led to a lower amount of CNT

distributed at the ceramic boundaries and, thus, a higher CNT nominal vol.% was needed to surpass the percolation threshold.

Remarkable electrical anisotropy was observed in all the composites, with higher conductivities in the direction perpendicular to the SPS pressing axis ($\sigma_\perp > \sigma_\parallel$). This is consequence of the preferential alignment of the CNTs in this direction, which enhances their interconnection. In a recent study, Kasperski *et al*[17] related the significant differences in the conductivity values published by authors using different measurement methods to this CNT preferential orientation. These authors pointed out that higher conductivities were reported when performing surface measurements along the bases of the sintered cylindrical pellets[6,30], in comparison with data obtained from measurements along the axis of the cylindrical pellets[17]. In the former case, data of $\sigma_\perp$ are reported, whereas $\sigma_\parallel$ is reported in the latter case.

It is worth mentioning that the CNT preferential alignment revealed by the electrical anisotropy in all the composites was only clearly observed in the microstructure of one of them (composite ST-stab, Fig. 5a), and it was revealed by the anisotropy of indentation crack length for three of them (composites ST-stab, ST-het and US-stab, table 3). Thus, the measurement of the electrical conductivity complements the microstructural and mechanical analysis, giving a more complete view of the MWNT distribution in the ceramic matrix.

The lower conductivity values, both $\sigma_\perp$ and $\sigma_\parallel$, obtained for the composites prepared with the MWNTs subjected to ultrasonic agitation during the acid treatment, $\sigma_\parallel = 0.3$ and $\sigma_\perp = 2.2$ $S \cdot m^{-1}$, and $\sigma_\parallel = 3.5$ $S \cdot m^{-1}$ and $\sigma_\perp = 8.6$ $S \cdot m^{-1}$, for the composites US-stab and US-het, respectively, (Table 3) reflect significant differences in the conduction percolation network in these composites in comparison with the ones prepared with MWNTs subjected to stirring during the functionalization treatment.

It is well established that there are two major contributions to the resistance of a CNT network[33,34]: the resistance of the carbon nanotube bundles and the resistance of the junctions between these bundles, being the latter contribution the highest resistance introduced in the system[35]. The conduction mechanism across these junctions in CNT composites has been successfully described in terms of fluctuation-induced electron tunnelling[32]. A CNT percolation network contains many conducting regions separated

by small insulating barriers, which are susceptible to charge fluctuations, and thus, to electric field fluctuations across the tunnelling junctions.

In this context, it is clear that in our study some structural damage or extensive shortening of the nanotubes has taken place during the functionalization routine including ultrasonic agitation[2,36]. This is in agreement with the observed microstructure using high magnification in SEM (Figs. 5g and 5h) where shorter MWNT bundles in comparison with the ones in the ST-stab and ST-het composites (Figs. 5e and 5f) were observed. The CNT shortening during the acid treatment assisted by ultrasonication has clearly modified the conduction percolation network in the composites US-stab and US-het. The existence of a higher number of junctions between the shorter CNT bundles after functionalization results in a higher resistivity of the composites. Kasperski *et al*[11] have also shown a decreased conductivity in Al_2O_3/CNT composites prepared with nanotubes subjected to covalent functionalization in nitric acid aqueous solution.

The composite powder colloidal processing routine also presents an influence on the conduction percolation network, and thus, on the electrical conductivity of the resulting composites. However, the effect is not as remarkable as the observed one for the two different acid treatment routines and is not clearly related to the CNT bundle length or the MWNT distribution through the matrix. As it can be observed in Table 3, lower electrical conductivity is obtained in the composite prepared with MWNTs subjected to stirring during the acid treatment when using the heterocoagulation technique to prepare the powder, in comparison with the one prepared using the charge stabilization technique. On the contrary, in the case of the composites prepared with the MWNTs subjected to ultrasonic agitation during the acid treatment, the highest conductivity values are obtained when using the heterocoagulation technique to prepare the powder.

The highest conductivity values achieved in this study are higher than reported values for 3YTZP/3.9 vol.% DWNT (double wall carbon nanotubes) composites, with 10 $S \cdot m^{-1}$ when measuring along the direction parallel to the SPS pressing axis ($\sigma_{\parallel}$)[17]. However, our values are lower than that reported one for Al_2O_3/2 vol.% MWNT[16], 100 $S \cdot m^{-1}$ when measuring along the direction perpendicular to this axis ($\sigma_{\perp}$). These differences in conductivity values could be explained by considering that different types of MWNTs are used in the different studies. A remarkable influence of the number of

layers and length on conductivity has been reported for 3YTZP/MWNT composites with ~3.5 MWNT vol.%. Whereas a conductivity of 100 $S \cdot m^{-1}$ was obtained when using nanotubes with 8 walls and 1.5 μm length, a value of 32 $S \cdot m^{-1}$ was reported for the composite prepared with nanotubes with 20 walls and length over 10 μm[11]. This fact, together with other factors that could influence the electrical conductivity in these composites, such as CNT damage or degree of bundling[17], must be considered in order to establish an adequate comparison with literature.

4. Conclusions.

The studied 3YTZP/MWNT composites are highly densified, with zirconia matrix presenting mainly tetragonal phase, and show a rather homogeneous microstructure with most of the MWNTs well dispersed at the zirconia grain boundaries. CNT agglomeration is only observed in one of the composites, after using the processing routine which involves the use of ultrasonic agitation during MWNT acid treatment and further heterocoagulation during MWNTs and ceramic powder mixing. No remarkable deterioration of the CNT structure during the acid treatment or spark plasma sintering was observed for any composite. However, long time MWNT suspension sonication with a high energy probe promoted graphitization of the nanotubes.

Whereas a patterned microstructure with MWNT bundles distributed surrounding circular CNT-free regions is observed in the composites prepared with the MWNT subjected to stirring during the acid treatment, such microstructure is not observed when using the MWNTs subjected to sonication during the acid treatment as a consequence of the existence of shorter and not interconnected MWNT bundles.

Although hardness of the composites is not remarkably dependent on the processing routine, significant differences are observed in the fracture behavior of the different composites. The anisotropy in the lengths of the cracks generated by Vickers indentation reveals a preferential alignment of the CNT bundles in the direction perpendicular to the SPS loading axis. Moreover, this anisotropy shows the role of these CNT bundles as preferential fracture paths in this direction. On the contrary, the shorter fracture length in the direction parallel to the SPS loading axis is due to fracture

deviation following a more tortuous path of the unaligned CNT bundles. The absence of this anisotropy in the composite prepared with the MWNTs subjected to ultrasonication during the acid treatment and further heterocoagulation is a consequence of the shorter CNT bundles without significant preferential orientation.

The remarkable electrical anisotropy observed in all the composites points to a preferential orientation of the CNT bundles in the direction perpendicular to the SPS loading axis. The lower conductivity values in the composites prepared with the MWNTs subjected to acid treatment including ultrasonic agitation is a consequence of the shortening of the CNTs during this treatment.

Our results indicate that the best processing routine for obtaining highly conductive 3YTZP/MWNT composites with homogeneous microstructure is the one which combines MWNT stirring during the acid treatment and further powder processing by charge stabilization.

Acknowledgments

The authors acknowledge the financial support provided by the Spanish Ministerio de Economía y Competitividad, under project MAT2015-67889-P, cofunded by European FEDER fundings. XRD and microscopy studied were performed at CITIUS facilities (Universidad de Sevilla).

Figure captions

Figure 1. X- ray diffraction patterns of the composites.

Figure 2. Raman spectra of the as-received MWNTs and the MWNTs subjected to the two different acid treatment routines. The spectra were normalized to the G band for easier comparison.

Figure 3. Raman spectra of the sintered composites prepared with (a) MWNT-ST and (b) MWNT-US. Raman spectra of the two different acid-treated MWNTs were included for comparison.

Figure 4. HRSEM micrographs of fracture surfaces of composites denoted as (a) ST-Stab, (b) ST-Het, (c) US-Stab and (d) US-Het.

Figure 5. Backscattered electron scanning (BSE) microscopy images from the composites cross sections, showing dark MWNT distributed throughout the matrix and some agglomerates (arrowed). (a), (b), (c) and (d) correspond to low magnification images; (e), (f), (g) and (h) correspond to higher magnification images. (a) and (e) ST-Stab, (b) and (f) ST-Het, (c) and (g) US-Stab and (d) and (h) US-Het. SPS pressing axis is indicated in (a) by arrows.

Figure 6. SEM micrographs illustrating typical Vickers indentations and crack paths on cross section surfaces of the composites denoted as (a) ST-Stab, (b) ST-Het, (c) US-Stab and (d) US-Het. SPS pressing axis is indicated in (a) by arrows.

Figure 7. Fracture crack originated in ST-Stab composite by Vickers indentation in the directions perpendicular (a) and parallel (b) to the SPS pressing axis. (c) High resolution SEM image showing a single CNT bundle bridging a crack.

References

[1] Q. Zhang, J.Q. Huang, W.Z. Qian, Y.Y. Zhang, F. Wei, The road for nanomaterials industry: A review of carbon nanotube production, post-treatment, and bulk applications for composites and energy storage, Small 9 (2013) 1237–1265.

[2] R. Poyato, A.L. Vasiliev, N.P. Padture, H. Tanaka, T. Nishimura, Aqueous colloidal processing of single-wall carbon nanotubes and their composites with ceramics, Nanotechnology 17 (2006) 1770–1777.

[3] M. Poorteman, M. Traianidis, G. Bister, F. Cambier, Colloidal processing, hot pressing and characterisation of electroconductive MWCNT–alumina composites with compositions near the percolation threshold, J. Eur. Ceram. Soc. 29 (2009) 669–675.

[4] A. Morales-Rodríguez, A. Gallardo-López, A. Fernández-Serrano, R. Poyato, A. Muñoz, A. Domínguez-Rodríguez, Improvement of Vickers hardness measurement on SWNT/Al_2O_3 composites consolidated by spark plasma sintering, J. Eur. Ceram. Soc. 34 (2014) 3801–3809.

[5] X. Wang, N Padture, H. Tanaka, Contact-damage-resistant ceramic/single wall carbon nanotubes and ceramic/graphite composites. Nat. Mater. 3 (2004) 539-544.

[6] T. Ukai, T. Sekino, A. Hirvonen, N. Tanaka, T. Kusunose, T. Nakayama, et al. Preparation and electrical properties of carbon nanotubes dispersed zirconia nanocomposites, Key. Eng. Mater. 317-318 (2006) 661–664.

[7] A.M. Zahedi, J. Javadpour, H.R. Rezaie, M. Mazaheri, Analytical study on the incorporation of zirconia-based ceramics with carbon nanotubes: Dispersion methods and mechanical properties, Ceram. Int. 42 (2016) 1653-1659.

[8] A. Peigney, C. Laurent, E. Flahaut, A. Rousset, Carbon nanotubes in novel ceramic matrix nanocomposites, Ceram. Int. 26 (2000) 577-683.

[9] A. Datye, KH Wu, G. Gomes, V. Monroy, HT Lin, J. Vleugels et al. Synthesis, microstructure and mechanical properties of yttria stabilized zirconia (3YTZP)-multi-walled nanotube (MWNTs) nanocomposite by direct in-situ growth of MWNTs on zirconia particles, Compos. Sci. Technol. 70 (2010) 2086-2092.

[10] J. González-Julián, P. Miranzo, M. I. Osendi, M. Belmonte, Carbon nanotubes functionalization process for developing ceramic matrix nanocomposites, J. Mater. Chem. 21 (2011) 6063-6071.

[11] A. Kasperski, A. Weibel, C. Estournès, Ch. Laurent, A. Peigney, Multi-walled carbon nanotube-Al_2O_3 composites: Covalent or non-covalent functionalization for mechanical reinforcement, Scripta Mater. 75 (2014) 46-49.

[12] M. Estili, A. Kawasaki, An approach to mass-producing individually alumina-decorated multi-walled carbon nanotubes with optimized and controlled compositions, Scripta Mater. 58 (2008) 906-909.

[13] M. Estili, A. Kawasaki, H. Sakamoto, Y. Mekuchi, M. Kuno, T. Tsukada, The homogeneous dispersion of surfactantless, slightly disordered, crystalline, multiwalled carbon nanotubes in α-alumina ceramics for structural reinforcement, Acta Mater. 56 (2008) 4070-4079.

[14] J. Yi, T. Wang, Z. Xie, W. Xue, Zirconia-based nanocomposite toughened by functionalized multi-wall carbon nanotubes, J. All. Comp. 581 (2013) 452-458.

[15] J. Yi, W. Xue, T. Wang, Z. Xie, Mechanical and electrical properties of chemically modified MWCNTs/3Y-TZP composites, Ceram. Inter. 41 (2015) 9157-9162.

[16] W. Wang, G. Yamamoto, K. Shirasu, Y. Nozaka, T. Hashida, Effects of processing conditions on microstructure, electrical conductivity and mechanical properties of MWCNT/alumina composites prepared by flocculation, J. Eur. Ceram. Soc. 35 (2015) 3903-3908.

[17] A. Kasperski, A. Weibel, D. Alkattan, C. Estournès, Ch. Laurent, A. Peigney, Double-walled carbon nanotube/zirconia composites: Preparation by spark plasma sintering, electrical conductivity and mechanical properties, Ceram. Int. 41 (2015) 13731-13738.

[18] J. Sun, L. Gao, W. Li, Colloidal processing of carbon nanotube/alumina composites, Chem. Mater. 14 (2002) 5169–5172.

[19] J.P. Fan, D.Q. Zhao, M.S. Wu, Z.N. Xu, J. Song, Preparation and microstructure of multi-wall carbon nanotubes-toughened Al_2O_3 composite, J. Am. Cerm. Soc. 89 (2006) 750–753.

[20] R. Poyato, A. Gallardo-López, F. Gutiérrez-Mora, A. Morales-Rodríguez, A. Muñoz, A. Domínguez-Rodríguez, Effect of high SWNT content on the room temperature mechanical properties of fully dense 3YTZP/SWNT composites, J. Eur. Ceram. Soc. 34 (2014) 1571-1579.

[21] R. Poyato, J. Macías-Delgado, A. Gallardo-López, A. Muñoz, A. Domínguez-Rodríguez, Microstructure and impedance spectroscopy of 3YTZP/SWNT ceramic nanocomposites, Ceram. Int. 41 (2015) 12861-12868.

[22] A. Gallardo-López, A. Morales-Rodríguez, J. Vega-Padillo, R. Poyato, A. Muñoz, A. Domínguez-Rodríguez, Enhanced carbon nanotube dispersion in 3YTZP/SWNTs composites and its effect on room temperature mechanical and electrical properties, J. Alloys Comp. 682 (2016) 70-79.

[23] Q. Chen, S. Debnath, E. Gregan, H.J. Byrne, Ultrasound-assisted SWNTs dispersion: effects of sonication parameters and solvent properties, J. Phys. Chem. C 114 (2010) 8821-8827.

[24] A. S. Paipetis, Stress Induced Changes in the Raman Spectrum of Carbon Nanostructures and their Composites. In "Carbon nanotube enhanced aerospace composite materials", A.S. Paipetis and V. Kostopoulos (eds), Springer (2012) 185-212.

[25] K.E. Thomson, D. Jiang, W. Yao, R.O. Ritchie, A.K. Mukherjee, Characterization and mechanical testing of alumina-based nanocomposites reinforced with niobium and/or carbon nanotubes fabricated by spark plasma sintering, Acta Mater. 60 (2012) 622–632.

[26] A. Kasperski, A. Weibel, D. Alkattan, C. Estournes, V. Turq, Ch. Laurent, A. Peigney, Microhardness and friction coefficient of multi-walled carbon nanotube-yttria-stabilized ZrO_2 composites prepared by spark plasma sintering. Scripta Mater. 69 (2013) 338–341.

[27] M. Mazaheri, D. Mari, R. Schaller, G. Bonnefont, G.Fantozzi, Processing of yttria stabilized zirconia reinforced with multi-walled carbon nanotubes with attractive mechanical properties, J. Eur. Ceram. Soc. 31 (2011) 939-945.

[28] I. Ahmad, B. Yazdani, Y. Zhu, Recent advances on carbon nanotubes and graphene reinforced ceramics nanocomposites, Nanomat. 5 (2015) 90-114.

[29] C. Balázsi, A. Kónya, F. Wéber, L.P. Biró, P. Arató, Preparation and characterization of carbon nanotube reinforced silicon nitride composites, Mater. Sci. Eng. C 23 (2003) 1133-1137.

[30] J.H. Shin, S.H. Hong, Microstructure and mechanical properties of single wall carbon nanotube reinforced yttria stabilized zirconia ceramics, Mater. Sci. Eng. A 556 (2012) 382-387.

[31] S.L. Shi, J. Liang, Effect of multiwall carbon nanotubes on electrical and dielectric properties of yttria-stabilized zirconia ceramic, J. Am. Ceram. Soc. 89 (2006) 3533–3535.

[32] S.L. Shi, J. Liang, Electronic transport properties of multiwall carbon nanotubes/yttria stabilized zirconia composites, J. Appl. Phys. 101 (2007) 023708.

[33] S.G. Louie, Electronic properties, junctions, and defects of carbon nanotubes. In: "Carbon nanotubes: synthesis, structure, properties, and applications", Topics in applied physics vol. 80. M.S. Dresselhaus, G. Dresselhaus, P. Avouris (eds). Springer (2001) 113-145.

[34] P.N. Nirmalraj, P.E. Lyons, S. De, J.N. Coleman, J.J. Boland, Electrical connectivity in single-walled carbon nanotube networks, Nano Lett. 9 (2009) 3890–3895.

[35] C. Li, E.T. Thostenson, T.W. Chou, Dominant role of tunneling resistance in the electrical conductivity of carbon nanotube-based composites, Appl. Phys. Lett. 91 (2007) 223114.

[36] Liu J et al, Fullerene pipes, Science 280 (1998) 1253–1256.

Table 1. Processing routines followed in this study

Compote	MWNT acid treatment agitation procedure		MWNT tip sonication time		pH conditions during composite powder mixing		Slurry drying	
	ultrasonic agitation	stirring	15 min	45 min	Basic	Acid	Hot plate	Lyophilization
ST-stab		x	x		x		x	
ST-het		x	x			x		x
US-stab	x		x		x		x	
US-45-stab	x			x	x		x	
US-het	x		x			x		x

Table 2. Experimental and relative densities, grain size and Raman I_D/I_G ratio of the composites.

Composite	ρ (g·cm^{-3}) ± 0.1	ρ_{rel} (%) ± 2	d (nm)	I_D/I_G	I_D/I_G range (min-max)
ST-stab	5.8	96.7	227 ± 16	0.83 ± 0.09	(0.74-0.93)
ST-het	5.9	98.3	207 ± 15	1.03 ± 0.26	(0.73-1.26)
US-stab	6.0	100	228 ± 12	0.94 ± 0.16	(0.83-1.16)
US-het	5.8	97.4	226 ± 36	0.89 ± 0.09	(0.77-0.95)

Table 3. Vickers hardness (H_v), crack length and electrical conductivity (σ) of the composites.

Composite	H_v (GPa)		Crack length (μm)		σ (S·m^{-1})	
	i.p. surface	c.s. surface	Parallel direction	Perpendicular direction	$\sigma_{\parallel}$	$\sigma_{\perp}$
ST-stab	10.9 ± 0.4	10.86 ± 0.20	42 ± 5	80 ± 9	16.4	28.8
ST-het	12.2 ± 0.4	12.25 ± 0.14	46 ± 5	60 ± 6	7.1	20.6
US-stab	12.60 ± 0.14	12.56 ± 0.24	41 ± 5	65 ± 9	0.3	2.2
US-het	12.5 ± 0.3	12.95 ± 0.19	52 ± 6	56 ± 5	3.5	8.6

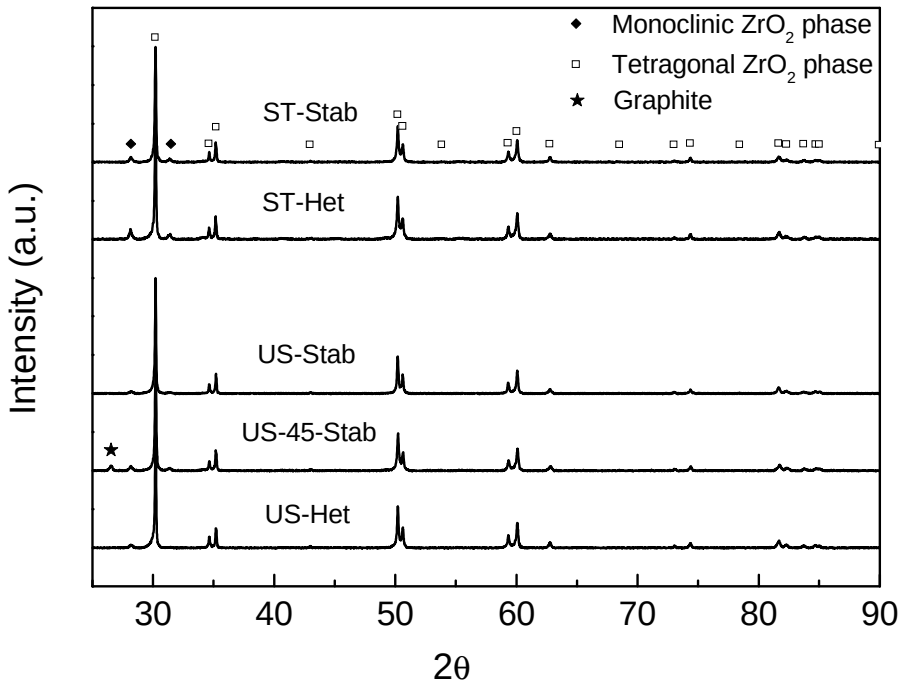
Monoclinic ZrO2 phase
Tetragonal ZrO2 phase
Graphite
ST-Stab
ST-Het
US-Stab
US-45-Stab
US-Het
Intensity (a.u.)
30
40
50
60
70
80
90
2θ

Figure 1

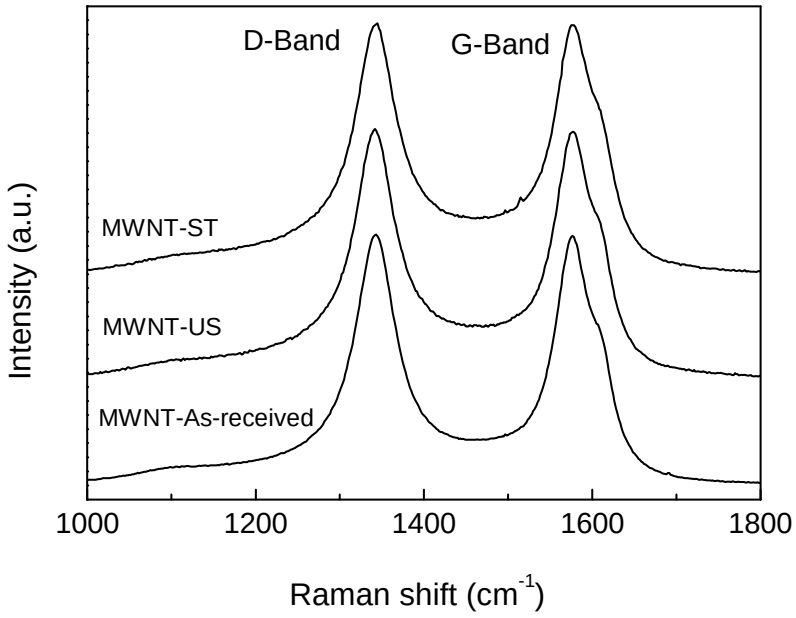
D-Band
G-Band
MWNT-ST
MWNT-US
MWNT-As-received
Intensity (a.u.)
1000
1200
1400
1600
1800
Raman shift (cm-1)

Figure 2

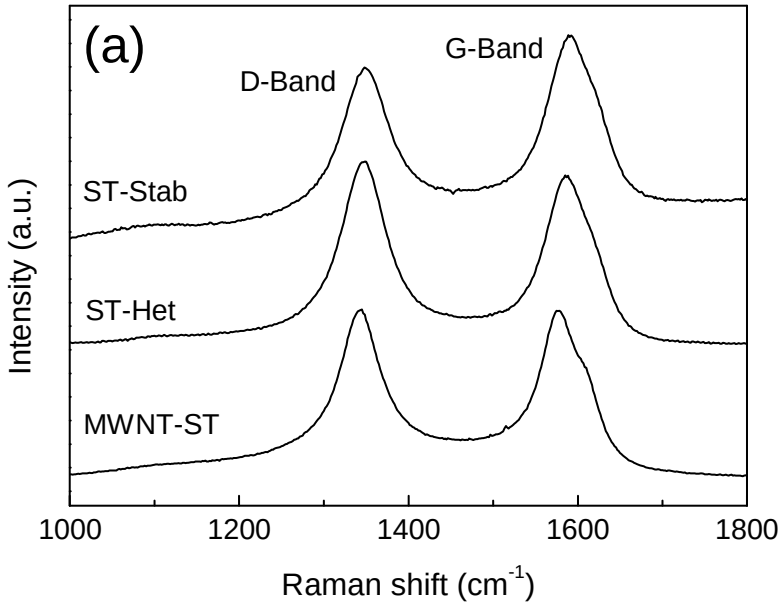
(a)
D-Band
G-Band
ST-Stab
ST-Het
MWNT-ST
Intensity (a.u.)
1000
1200
1400
1600
1800
Raman shift (cm-1)

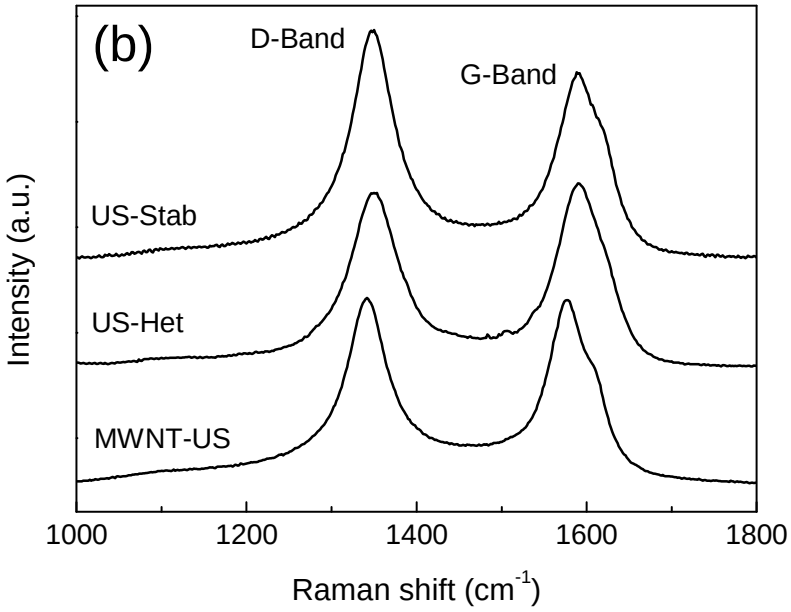
(b)
D-Band
G-Band
US-Stab
US-Het
MWNT-US
Intensity (a.u.)
1000
1200
1400
1600
1800
Raman shift (cm-1)

Figure 3

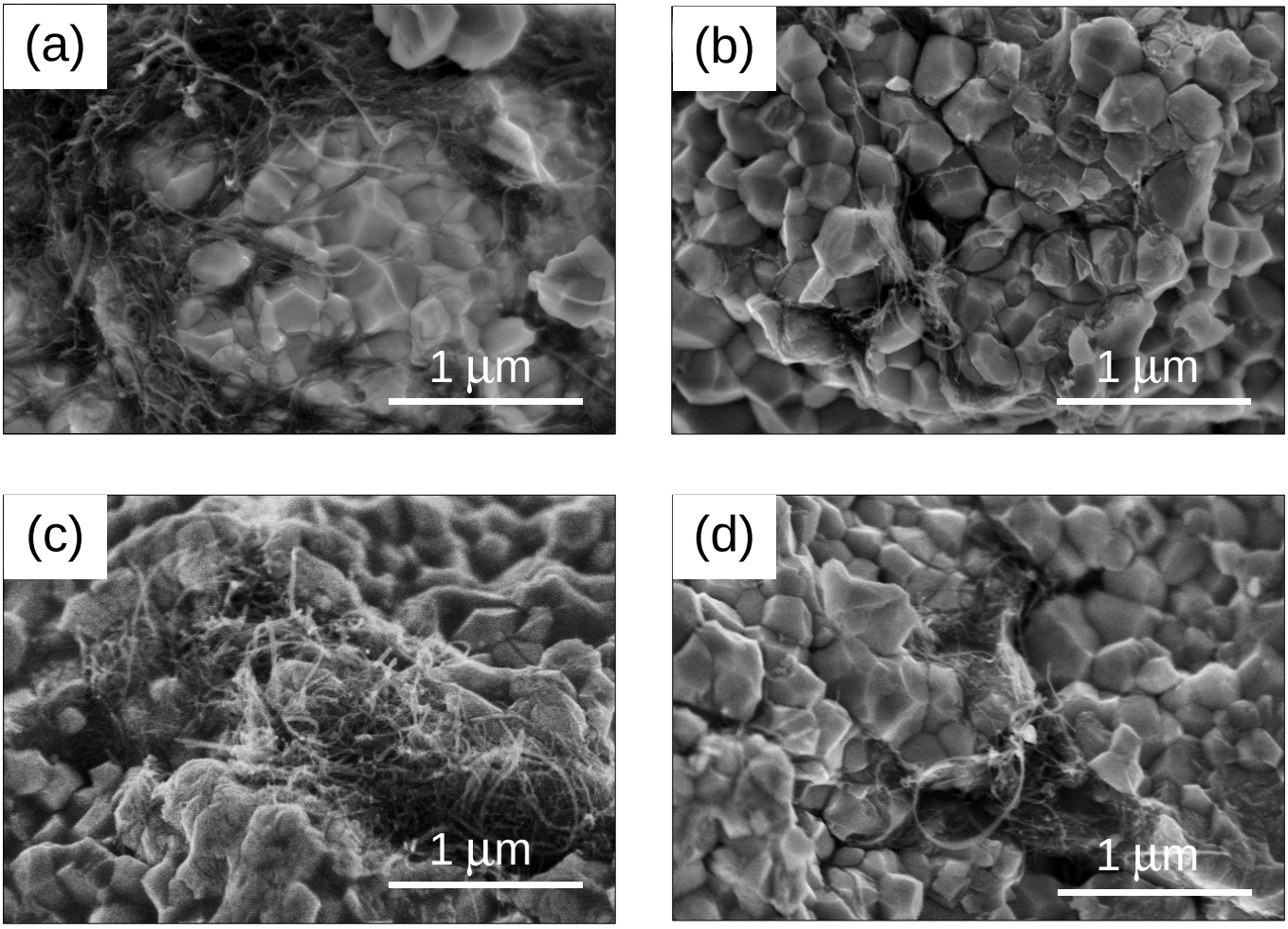

Figure 4

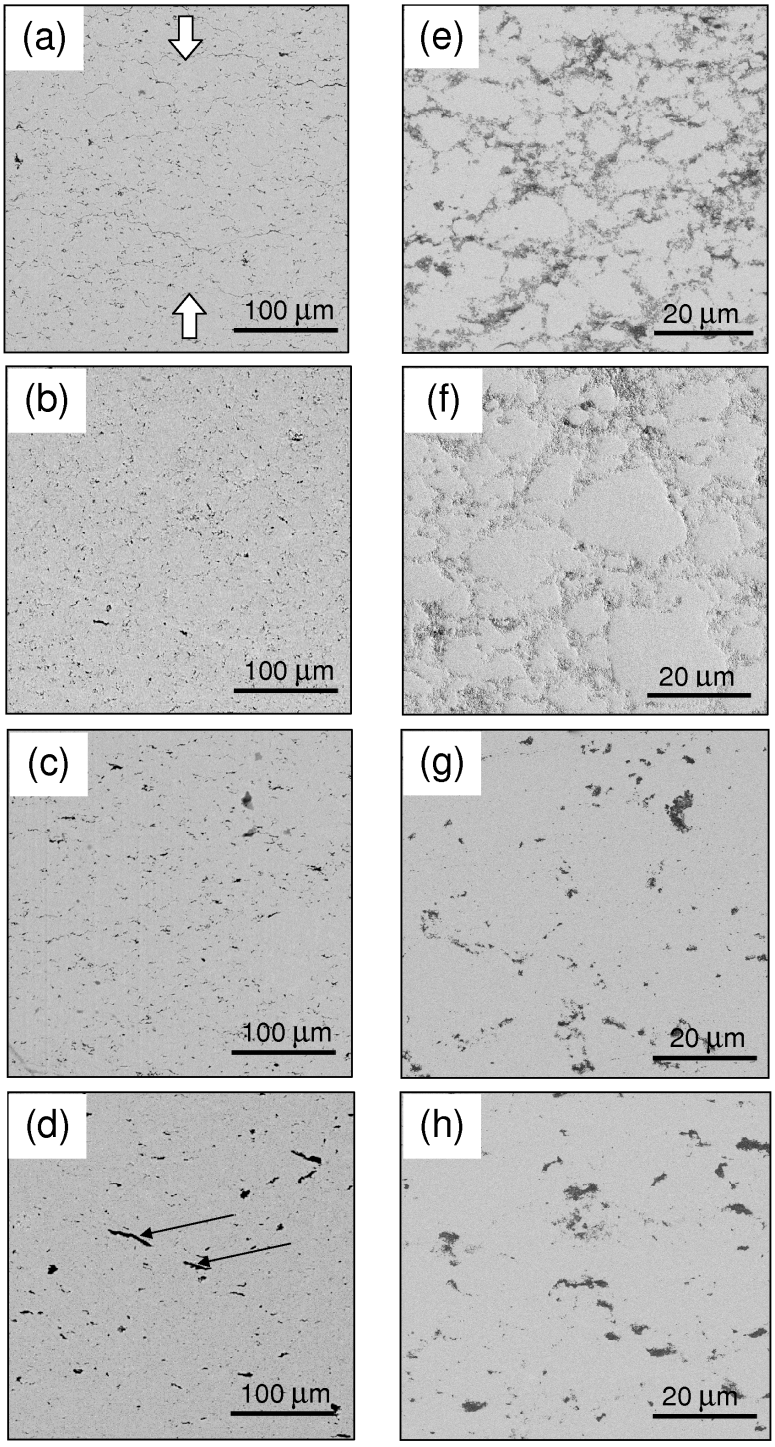

Figure 5

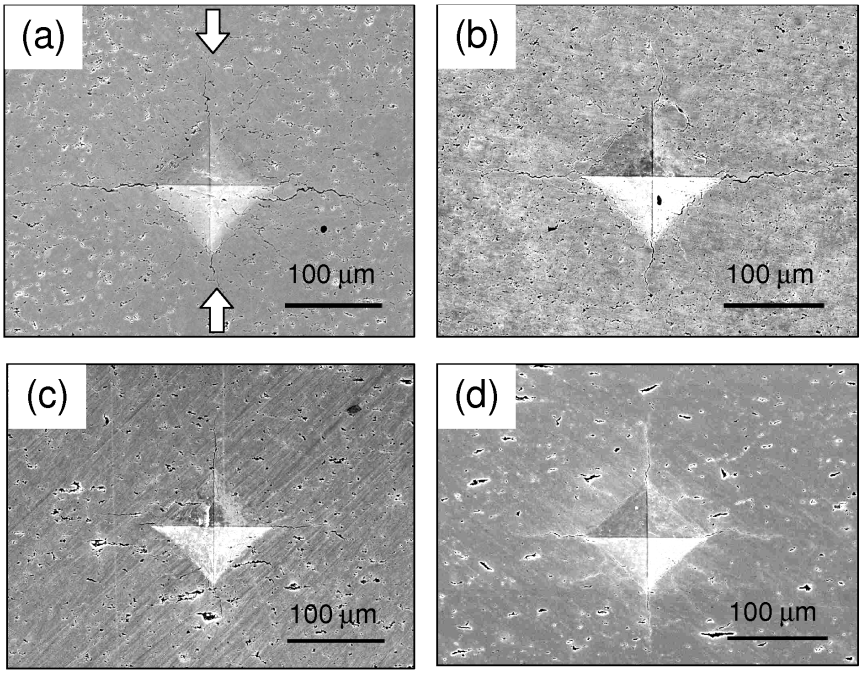

Figure 6

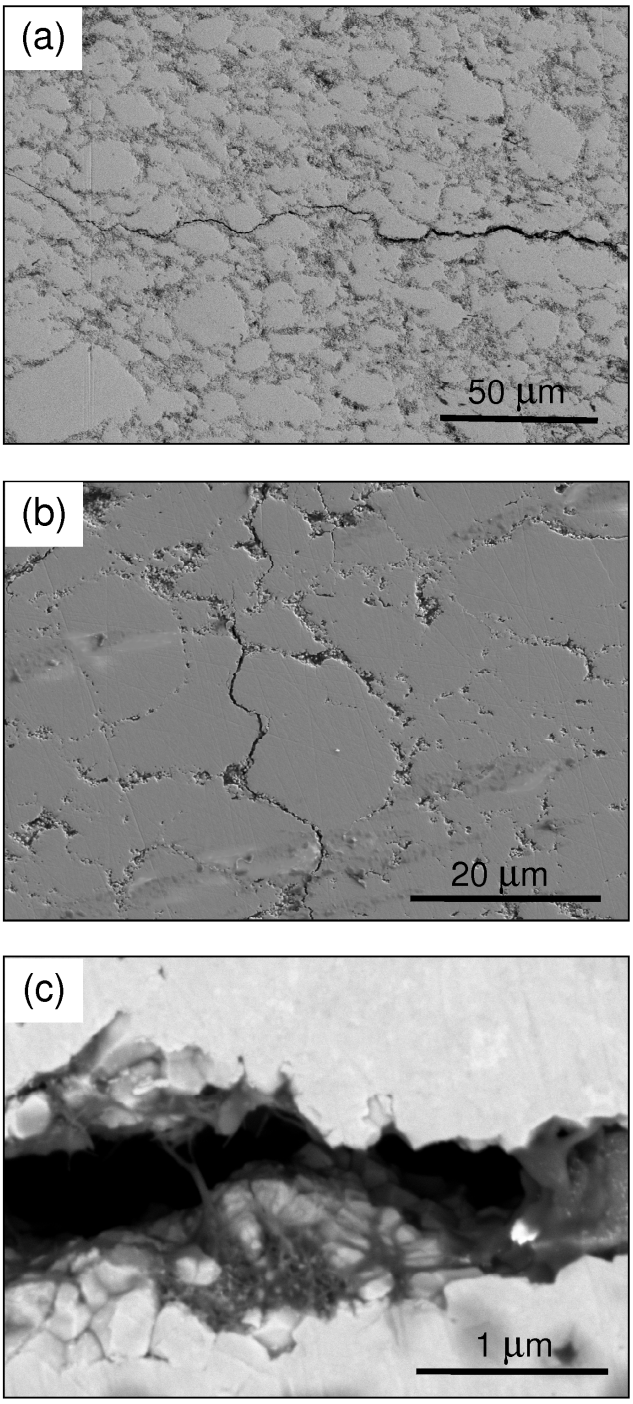

Figure 7